



Transient stability analysis of DFIG-based wind farm-integrated power system considering gearbox ratio and reactive power control

Shabani, Hamid Reza; Hajizadeh, Amin; Kalantar, Mohsen; Lashgari, Mahmoud; Nozarian, Mahdi

Published in:
Electrical Engineering

DOI (link to publication from Publisher):
[10.1007/s00202-023-01906-3](https://doi.org/10.1007/s00202-023-01906-3)

Creative Commons License
CC BY 4.0

Publication date:
2023

Document Version
Publisher's PDF, also known as Version of record

[Link to publication from Aalborg University](#)

Citation for published version (APA):
Shabani, H. R., Hajizadeh, A., Kalantar, M., Lashgari, M., & Nozarian, M. (2023). Transient stability analysis of DFIG-based wind farm-integrated power system considering gearbox ratio and reactive power control. *Electrical Engineering*, 105, 3719-3735. <https://doi.org/10.1007/s00202-023-01906-3>

General rights

Copyright and moral rights for the publications made accessible in the public portal are retained by the authors and/or other copyright owners and it is a condition of accessing publications that users recognise and abide by the legal requirements associated with these rights.

- Users may download and print one copy of any publication from the public portal for the purpose of private study or research.
- You may not further distribute the material or use it for any profit-making activity or commercial gain
- You may freely distribute the URL identifying the publication in the public portal -

Take down policy

If you believe that this document breaches copyright please contact us at vbn@aub.aau.dk providing details, and we will remove access to the work immediately and investigate your claim.



Transient stability analysis of DFIG-based wind farm-integrated power system considering gearbox ratio and reactive power control

Hamid Reza Shabani¹ · Amin Hajizadeh¹ · Mohsen Kalantar² · Mahmoud Lashgari² · Mahdi Nozarian³

Received: 16 April 2023 / Accepted: 14 June 2023 / Published online: 7 July 2023
© The Author(s) 2023

Abstract

Nowadays, integration of large-scale wind farms (WFs) into power systems is experiencing rapid growth. As this rapid integration can affect transient stability significantly, employing doubly fed induction generator (DFIG)-based wind turbines, which have shown better behavior regarding system stability, has attracted much attention. This research contributes to the literature by investigating the transient stability of the power system with increasing penetration of DFIG-based WF. In the proposed framework, the current-balance form is utilized for the network equations, and in this way, transient stability is performed using time-domain simulation. According to the simulation results, when the rate of wind power generation exceeds 0.7 per-unit, the increasing trend of the critical clearing time (CCT) is reversed and the CCT decreases greatly with the increased wind power penetration. In addition, the reactive power compensation by DFIG, the gearbox ratio, the power system strength, and DFIG parameters are comprehensively investigated as effective parameters on transient stability. Since the rated rotor speed of DFIG significantly impacts the electrical torque and machine currents, the reduction of the rated rotor speed due to the change of the gearbox ratio has been investigated as one of the effective factors to improve the transient stability. The simulation results demonstrate the effectiveness of the proposed approach in improving power system transient stability.

Keywords Transient stability assessment · Doubly fed induction generator · Gearbox ratio · Reactive power · Critical clearing time

List of symbols

η	TSI symbol	$V_s \angle \theta_s$	Magnitude and angle of the infinite bus terminal voltage
ρ_{\max}	Maximum angle separation	R	Blade length
$V_D + jV_Q$	Real and imaginary parts of voltage magnitude on DQ -axis	P_{tw}, T_{tw}	Extracted power and torque of the wind turbine
$V_{tSG} \angle \theta_{tSG}$	Magnitude and angle of the terminal voltage of SG	ρ	Air density
$V_d + jV_q$	Real and imaginary parts of voltage magnitude on dq -axis	X_{tot}	Total reactance
		$V_{ds} + jV_{qs}$	Real and imaginary parts of stator voltage magnitude of DFIG on dq -axis
		C_p	Performance coefficient
		$P_t + jQ_t$	Total active and reactive power
		β	Blade angle
		$V_{dr} + jV_{qr}$	Real and imaginary parts of rotor voltage magnitude of DFIG on dq -axis
		V_w	Wind speed
		λ_s	Stator flux
		ω_t	Speed of the wind turbine
		ω_{elB}	Electrical base speed
		r_s	Stator resistance (DFIG)
		$\omega_{r, rated}$	Rated rotor speed of DFIG

✉ Hamid Reza Shabani
h_shabani@alumni.iust.ac.ir

¹ Department of Energy Technology, Aalborg University, Esbjerg, Denmark

² Department of Electrical Engineering, Iran University of Science and Technology (IUST), Tehran, Iran

³ Faculty of Electrical Engineering, K.N. Toosi University of Technology, Tehran, Iran

ω_r	DFIG rotor speed
SG	Synchronous generators
DFIG	Doubly fed induction generator
SI	Simultaneous implicit
CCT	Critical clearing time
RSC	Rotor side converter
P_{ag}	Air gap power
S_B	Base MVA
$i_{dt} + ji_{qt}$	Real and imaginary <i>parts</i> of total current magnitude of DFIG on <i>dq</i> -axis
I_{GSC}	Grid-side convertor current
$i_{ds} + ji_{qs}$	Real and imaginary <i>parts</i> of stator current magnitude of DFIG on <i>dq</i> -axis
$e'_d + je'_q$	Real and imaginary <i>parts</i> of internal voltage magnitude of DFIG on <i>dq</i> -axis
L_m	Mutual inductance (DFIG)
λ_{opt}	Tip speed ratio (C_p is $C_{p,max}$, = 8.10)
$C_{p,max}$	Maximum value of C_p (β is 0° , = 0.48)
R_s	Stator resistance (SG)
$P_{GSC} + jQ_{GSC}$	Active and reactive power of grid-side convertor
λ	Tip speed ratio
$Q_{tot}(Q_{DFIG})$	Total reactive power (DFIG)
r_r	Rotor resistance (DFIG)
$V_{tD}\angle\theta_{tD}$	Magnitude and angle of the terminal voltage of DFIG
P_r	Active power of rotor (DFIG)
n_{gb}	Gearbox ratio
$P_{tw,rated}$	Nominal active power of wind turbine
Q_s	Reactive power of stator (DFIG)
L_{ss}, L_{rr}	Stator and rotor inductance (DFIG)
$\lambda_{dr}, \lambda_{qr}$	Stator flux of DFIG on <i>dq</i> -axis
$\lambda_{ds}, \lambda_{qs}$	Rotor flux of DFIG on <i>dq</i> -axis
WPP	Wind power penetration
TSA	Transient stability assessment
T-D	Time-domain
DAE	Differential–algebraic equation
GSC	Grid-side converter

1 Introduction

Electricity generation based on fossil fuel power stations can be considered as one of the largest sources of emissions. This challenge promoted the importance of renewable units integration as they can create a net-zero-emissions energy system [1]. Emerging transmission and distribution systems based on renewable energies have many environmental and economic advantages compared to traditional systems due to the intermittent nature of their production sources [2–4]. Also, due to the coordinated operation of many infrastructures, energy

hub systems based on renewable energies increase energy efficiency in addition to reducing emissions [5–9]. Meanwhile, wind turbines have penetrated more rapidly compared to other renewable resources [10–12]. According to the latest report of the Global Wind Energy Council, the global wind industry had its second-best year in 2021, with almost 94 GW of capacity added globally, trailing behind the 2020's record growth by only 1.8%. This brings total installed wind capacity to 837 GW, a growth of 12.4% compared to 2020 [13].

Transient stability, which is defined system's ability to maintain synchronism in a disturbance, has been assessed by considering synchronous generators (SGs) in different studies in the literature. In a disturbance state in the system where the wind power penetration (WPP) is not considerable, wind farms (WFs) are disconnected from the power system when the fault occurs. However, due to the increasing the WPP in the power systems, the study of their behavior and interaction with other power generation equipment and loads seems important [14, 15]. Analyzing the performance of the power system when dealing with dynamic and transient phenomena is one of the most significant issues in this field. As a result, this topic has been noticed by researchers and various studies have examined the effects of the high penetration of doubly fed induction generator (DFIG)-based WFs on the dynamic behavior of the power system and transient stability in recent decades.

In recent years, transient stability analysis of WFs integrated power systems has received increasing attention in terms of power system topologies, wind power generation technologies, fault types, and location as well as innovative models, methods, and approaches [16–23]. In this way, innovative frameworks follow the transient stability enhancement of a wind-penetrated power system through the power loss index method and the self-sorting analytical approach [16], Gauss–Hermite integral-based multi-point estimation method [17], two-stage model [18], supervisory adaptive predictive control [19], hybrid adaptive control of flywheel energy storage units [20], aggregated model [21], data-driven self-tuning additional sliding mode controller [22], and practical unit commitment framework constrained by the requirement of converter-driven stability [23].

Furthermore, from the existing wind power generation technologies, DFIG can be mentioned as a very attractive technology that has the most application in the industrial field. Accordingly, in the last decade, the transient stability analysis in power systems with the high penetration of DFIG-based WFs has become an interesting field of research [24–35]. As the first performed research in this field, in [24], the simultaneous implicit (SI) based on time-domain (T-D) simulation has been used and a suitable model has been provided for transient stability assessment (TSA). Also, the

researchers in [25] have also examined the effect of neglecting stator transients in the DFIG model. Comparison of the integration a common SG with a DFIG in power system when a 3-phase fault occurs, as one of the first works performed in this field, has been considered [26]. Also, a comprehensive study has been performed in [27] that approves that DFIG-based WF integration improves the system response to small disturbances.

The current state of the art in this field focused on innovative models and approaches to improve transient stability in a WF equipped with DFIGs. Reference [28] uses a 9-bus system, integrated with a DFIG WFs, to analyze its behavior during disturbances, and [29] utilizes a 6-bus test system to analyze stability by stator-flux-oriented vector control approach for both stator- and rotor-side converter (RSC). A nonlinear control and unified power flow controller for transient stability improvement with transient energy function (TEF) also are proposed in [30]. Semi-aggregation method through a nonlinear integral backstepping control [31] and active diode bridge fault current limiter topology by limiting the torque transients, currents peak, drop, active and reactive powers, and terminal voltage [32], also can be utilized. Further, a coordination approach to damp out the oscillations in a DFIG-integrated power system aiming at transient stability improvement using a power oscillation damper for static var compensator and power system stabilizer is developed in [33]. Reference [34] employs DFIG by TEF technique and super-twisting differentiator in the multi-machine power system to improve transient stability. TEF is also employed by [35] to detect real-time transient stability.

Furthermore, the authors in [36] investigate the transient stability of the DFIG-integrated power system using the phase-locked loop and establish the grid-connected system model. Reference [37] analyzes transient stability in the hydro-quebec system containing a DFIG-based WFs through the multilevel static synchronous compensator. A control topology that integrates the robust performance of fractional order sliding mode control with the high charging/discharging rate and low maintenance requirements of super-capacitors employed in a DFIG-based wind energy system aiming at transient stability improvement [38]. Reference [39] develops a noncontrolled fault current limiter model with reactive power support in a DFIG-integrated power system to enhance transient stability based on a non-superconducting reactor located on the rotor side. A new RSC control method is also proposed in [40], which utilizes DFIGs to improve stability and low-voltage ride-through (LVRT).

Considering various situations of the integration of DFIG WFs into the power systems, the reviewed studies have rarely been successful in compressive analyses of the transient behavior of the power systems in the presence of WFs, as the presented results in the above-mentioned literature are limited. The DFIG-based WF is very sensitive during the grid

faults. In the event of fault, the terminal voltage of DFIG decreases expressively from the rated voltage, and the RSC is highly effected due to injects of high fault current. Therefore, the performance of the DFIG under these conditions can considerably affect system stability [41]. In this way, it is very important to investigate a suitable method to enhance the stability and LVRT capability during the fault [42, 43]. Therefore, as the first work in this paper, the impact of Q_{DFIG} and P_{DFIG} has been investigated independently on improving the transient stability of the power system. According to the simulation results, when the rate of wind power generation exceeds 0.7 per-unit, the increasing trend of the critical clearing time (CCT) is reversed and the CCT decreases greatly with the increased WPP. Also, the generation of reactive power by DFIG has a desirable impact on transient stability. However, considering how DFIG supplies reactive power, the increased current in the rotor can be seen, leading to an increase in the converter rating. Thus, one of the solutions proposed in this paper to prevent the increase in the converter rating can be the use of external reactive power compensation devices in the DFIG bus. Furthermore, as the rated rotor speed in DFIG can be chosen arbitrarily by adjusting the gearbox ratio [44] and has a significant impact on the electrical torque and machine currents, the rated rotor speed is also analyzed as one of the factors affecting the transient stability improvement. Based on this, the reduction of the rated rotor speed due to the change of the gearbox ratio is investigated as one of the effective factors to improve the transient stability. In addition, the power system strength and DFIG parameters are comprehensively investigated as effective parameters on transient stability.

According to the above-mentioned points, the contributions of this paper can be summarized as follows:

- Using the current-balance form for the network equations and development of the grid-connected DFIG equivalent circuit for the dynamic studies of the power systems.
- Analysis of the effect of both P_{DFIG} (by changing the capacity of the WF equivalent machine) and Q_{DFIG} on transient stability improvement.
- Analysis of the effect of change in the rated rotor speed of DFIG by adjusting the gearbox ratio on transient stability improvement.
- Investigating the effect of the power system strength and DFIG parameters, specially DFIG stator resistance on power system transient stability.

The remaining parts of the paper are organized as follows: Section 2 provides power system components modeling and describes DFIG-based WF-integrated power system dynamic modeling. The simulation results are presented and discussed in Sect. 3, and finally, conclusions are drawn in Sect. 4.

2 DFIG-based WF-integrated power system dynamic modeling

2.1 DFIG components modeling

In power system stability analysis, the low-frequency dynamics over a time frame of 0.1–10 s after a fault are of interest [45]. Thus, fast dynamics that are damped out very quickly are ignored. Accordingly, in this paper, to analyze the transient stability, a two-axis model along with a static excitation system has been employed for SG [46]. The components of DFIG are aerodynamic system, drive-train system, induction generator, and power electronics converters. In this way, all parts of the DFIG are modeled, separately.

The wind turbine aerodynamic system has been usually represented by an algebraic model, and thus, for stability studies, its mechanical dynamics are ignored, Eq. (1) [47].

$$P_{tw} = (0.5)\rho\pi R^2 C_p(\lambda, \beta) V_w^3 \quad (1)$$

where

$$\lambda = (\omega_t \cdot R) / V_w \quad (2)$$

Also, in this paper, the blade angle pitch control has not been considered and the wind speed has been assumed to be constant, as in other works [11, 12, 27, 35, 48]. At any given wind speed, there is an optimal wind turbine speed, in which the power extracted from the wind turbine is maximum (λ_{opt} , $C_{p,max}$). Accordingly, by combining Eqs. (1) and (2), the equations of the wind turbine power and torque can be rewritten as Eqs. (3) and (4) [11].

$$P_{tw,max} = K_{opt}\omega_t^3 \quad (3)$$

$$T_{tw,max} = K_{opt}\omega_t^2 \quad (4)$$

where

$$K_{opt} = ((0.5)\rho\pi R^5 C_{p,max}) / \lambda_{opt}^3$$

The curve of speed-optimal torque (power) for DFIG is shown in Fig. 1. The rated wind speed is 15 m/s. According to Fig. 1 there are two different operating regimes for DFIG. In the sub-rated regime, the rated wind speed value is above the wind speed and the DFIG must follow the curve of maximum torque. However, in the rated regime, the rated wind speed value is below the wind speed and the speed and torque of the turbine must be limited to their rated values. The rated rotor speed can be chosen arbitrarily by adjusting the gearbox ratio, and the rated rotor speed has a significant impact on the electrical torque and machine currents, but due to the small amplitude, it has little impact on the rotor voltage [47].

Choosing higher rated rotor speed results in lower electrical torque because the torque is defined by Eq. (5):

$$T_{e,rated} = P_{ag,rated} / \omega_{r,rated} \quad (5)$$

Therefore, in terms of the converter rating, the higher value of rated rotor speed is better due to create less the amplitude of the machine currents. Thus, in the present paper, the rated rotor speed of DFIG has been considered equal to 1.2 per-unit. Also, according to experimental studies and power system simulations, a two-mass model is preferred for the drive-train system of the wind turbine when studying the stability [11, 47]. Thus, the two-mass drive-train model is used for DFIG in this paper.

Normally, the stator transients in asynchronous generators and SGs have not been considered for dynamic analysis of the power system. Therefore, the currents and voltages are represented as phasors in the transient stability simulation programs [49]. Accordingly, the stator transients are also ignored in this paper, and thus, the dynamic equations of the induction generator are expressed as follows (Eqs. (6–10)) [50].

$$V_{qs} = -r_s i_{qs} + e'_q - L'_s i_{ds} \quad (6)$$

$$V_{ds} = -r_s i_{ds} + e'_d + L'_s i_{qs} \quad (7)$$

$$\frac{1}{\omega_b} \frac{d}{dt} e'_d = \frac{1}{T_0} (-e'_d + (L_{ss} - L'_s) i_{qs}) + (1 - \omega_r) e'_q - \frac{L_m}{L_{rr}} V_{qr} \quad (8)$$

$$\frac{1}{\omega_b} \frac{d}{dt} e'_q = -\frac{1}{T_0} (e'_q + (L_{ss} - L'_s) i_{ds}) - (1 - \omega_r) e'_d + \frac{L_m}{L_{rr}} V_{dr} \quad (9)$$

where

$$T_e = e'_d i_{ds} + e'_q i_{qs},$$

$$e'_d = -\frac{L_m}{L_{rr}} \lambda_{qr} T_0 = \frac{L_{rr}}{R_r}, L'_s = \left(L_{ss} - \frac{L_m^2}{L_{rr}} \right), e'_q = \frac{L_m}{L_{rr}} \lambda_{dr} \quad (10)$$

Also, the electrical control system of DFIG consists of two parts: the RSC and the grid side converter (GSC). The objective of the RSC is to limit the rotor speed in the rated operating regime and to maximize the power extracted of the wind turbine in a sub-rated operating regime. On the other hand, the objective of the GSC is to always control the power factor and to keep the dc-link voltage constant [11, 47]. In terms of speed, the inner-loop current controllers of the power electronic converters are so fast compared with laboratory results, and theoretical considerations have shown that the speed operation of is much faster than the electromechanical transients studied in the stability analysis of the power system, and thus, their operation does not have a significant effect on the power system transient stability studies. In this way, a new reference current can be generated in 10 ms or

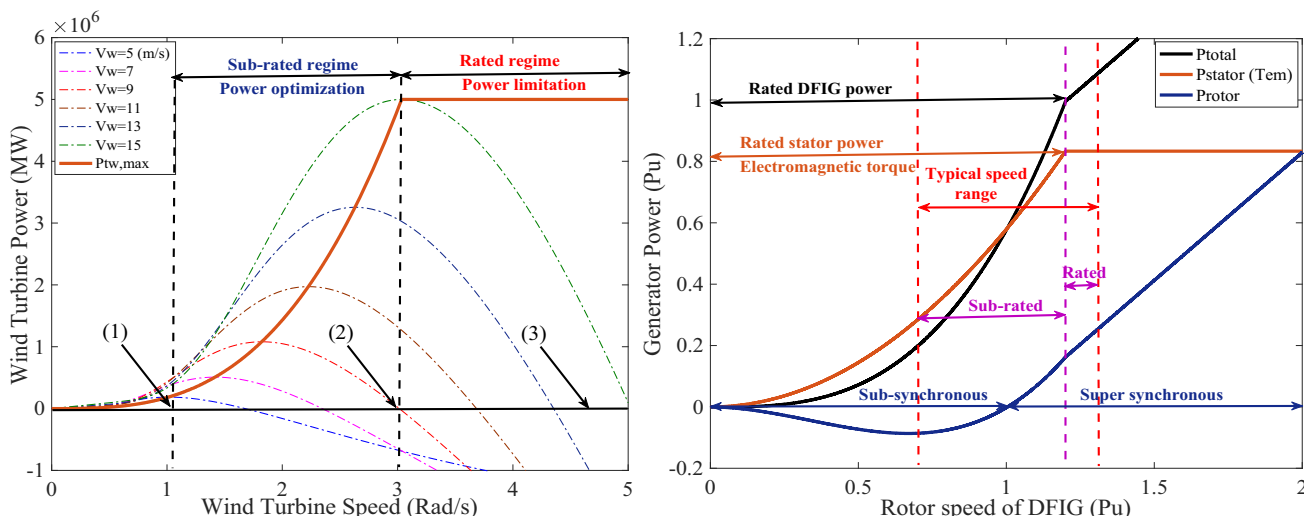


Fig. 1 Typical reference power (electromagnetic torque) based on the rotor speed

less, and it should be noted that 10 ms is a normal time step in power system dynamic simulations [12, 47, 51]. As a result, change in the current controllers can be considered instantaneous.

Accordingly, considering that the GSC controls are done instantaneously, the AC current of the GSC is such that the active power injected into the grid matches that of the RSC at the unity power factor. Therefore, the active power transfer of the rotor is made completely by the GSC, and the DC-link voltage remains constant [12]. Accordingly, it is assumed in this paper that the converters are ideal (the GSC is modeled as the current source and the RSC is modeled as the voltage source) and the DC-link voltage is constant.

According to what is said above, the model used for DFIG has been based on two basic assumptions: (1) electromagnetic transients in the stator and the branch between the inverters and the grid can be ignored. This assumption has no significant impact on electromechanical oscillations and helps to solve stator equations together with grid equations, and (2) it is assumed that the current control can be considered instantaneous, while the dynamics in the current control loops are ignored. The time constant of the current control is about one cycle (10 ms), which is quite faster than the time scale of transient stability studies (in the order of seconds). Therefore, the fast dynamics of such a control system have no impact on electromechanical oscillations.

2.2 The grid-connected DFIG modeling

When the way of connecting the machine to the grid is expressed, the network equations are extracted, and dynamic modeling is completed. It should be noted that the transient stability simulation is generally simplified using the differential–algebraic equation (DAE) model with network equations

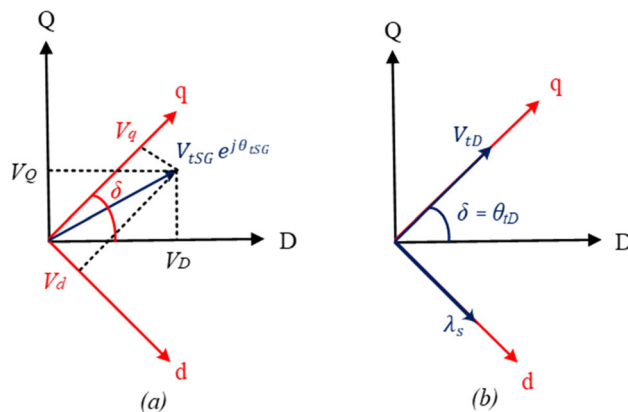


Fig. 2 The vector diagram of the machine (SG and DFIG) and grid reference frame

in the current-balance form because the network-admittance matrix should be refactored only when a disturbance is occurring [46]. In the same direction, Fig. 2 shows the vector diagram of how the synchronous reference frames of machines (the reference dq -frame) and the grid (the reference DQ -frame) are connected. Figure 2a shows the terminal voltage of the machine (SG) that is expressed in terms of the reference DQ -frame (Eq. (11)) [46].

$$V_{tSG} e^{j\theta_{tSG}} = (V_D + jV_Q) = (V_d + jV_q) e^{j(\delta - \frac{\pi}{2})} \tag{11}$$

Accordingly, the DAE model of the network equations in the current-balance form can be expressed as Eqs. (12) and (13) for SG [46].

$$R_s I_d - (X'_q + X_{tot}) I_q - E'_d + V_s \sin(\delta - \theta_s) = 0 \tag{12}$$

$$R_s I_q + (X'_d + X_{tot}) I_d - E'_q + V_s \cos(\delta - \theta_s) = 0 \tag{13}$$

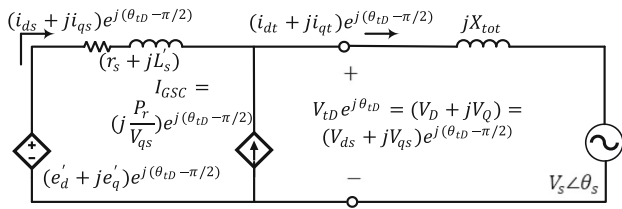


Fig. 3 DFIG equivalent circuit in the grid-connected condition for dynamic studies

Similarly, Fig. 2b shows the connection between dq -reference frame of DFIG and DQ-reference frame of the power system. Thus, the terminal voltage equation of DFIG is as follows (Eq. (14)):

$$V_{td} e^{j\theta_{td}} = (V_D + j V_Q) = (V_{ds} + j V_{qs}) e^{j(\delta - \pi/2)} \quad (14)$$

By using the classical vector control method for DFIG modeling [11], the DFIG stator flux is aligned with the d -axis. Therefore, $V_s = V_{ds} + j V_{qs}$, $V_{qs} = |V_s|$, $V_{ds} = 0$, and $\delta = \angle V_s$. In this way and according to the points expressed, the DFIG equivalent circuit in the grid-connected condition is presented in Fig. 3.

Therefore, the network equations in the current-balance form are obtained using the equivalent circuit developed for DFIG (Eqs. (15,16)).

$$-V_{qs} \cos\theta_{td} - \left(X_{tot} \left(i_{qs} + \frac{P_r}{V_{qs}} \right) \sin\theta_{td} \right) + (X_{tot} i_{ds} \cos\theta_{td}) + V_s \cos\theta_s = 0 \quad (15)$$

$$-V_{qs} \sin\theta_{td} + \left(X_{tot} \left(i_{qs} + \frac{P_r}{V_{qs}} \right) \cos\theta_{td} \right) + (X_{tot} i_{ds} \sin\theta_{td}) + V_s \sin\theta_s = 0 \quad (16)$$

3 Simulation results and analyses

In this paper, a single machine infinite bus (SMIB) system has been employed for TSA. To investigate the effect of WPP on power system transient stability, a WF is added to the base power system in the point of common connection (PCC) bus. It should be noted that as with other work done in this area [11, 12, 14, 35], the WF is modeled with aggregated wind turbines as an equivalent single machine. In this way and according to Sect. 2, the dynamic modeling of the power system can be represented using a set of DAEs.

$$\dot{x} = f(x, y, u) \quad (17)$$

$$0 = g(x, y, u) \quad (18)$$

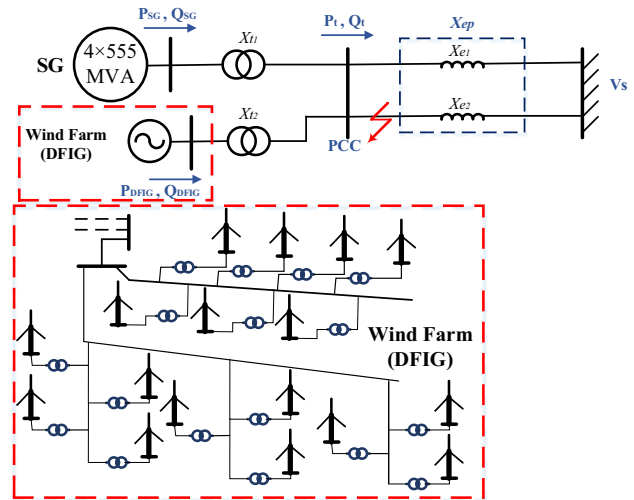


Fig. 4 The schematic of the SMIB system

where u is the system’s input and x and y , respectively, represent the state and algebraic variables. As a result, the function f represents the power system’s differential equations, while the function g represents its algebraic equations. The equations should be solved step-by-step in the time domain for investigating transient stability using a T-D simulation, making the SI method one of the best approaches [12]. In this approach, nonlinear differential equations are converted into nonlinear algebraic equations using trapezoidal numerical integration at each time-step, and the set of equations is then solved by the Newton–Raphson technique. It should be noted that the requirement for numerical simulation of a power system in the transient state is to calculate the initial conditions of the system variables that are obtained by load flow. Accordingly, employing the equivalent circuit of the DFIG and the power system, T-D simulation has been performed by MATLAB and the transient stability status is analyzed comprehensively. Figure 4 shows the power system under study that has been used in Ref. [12]. The parameters and base case operation of the power system are presented in Appendix. A.

3.1 DFIG WFs integration analyses

It is assumed that because of the fault (a three-phase short circuit in the line X_{e2}), the PCC bus voltage is decreased by 0.2 per-unit. In this paper, to analyze more accurately the impact of increasing WPP on the transient stability status, 3 cases have been studied. Thus, as the WPP in the power system increases, the capacity of the WF equivalent machine also changes and increases.

- Case A: DFIG WFs (aggregated model with capacity of 555 MW) to increase WPP by 15–30%.

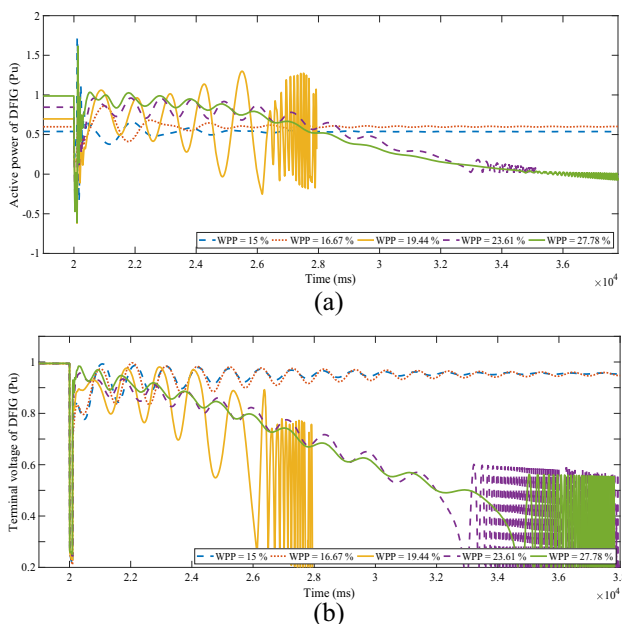


Fig. 5 The curve of the DFIG for Case A **a** the active power and **b** the terminal voltage

- Case B: DFIG WFs (aggregated model with capacity of 1110 MW) to increase WPP by 30–60%.
- Case C: DFIG WFs (aggregated model with capacity of 2220 MW) to increase WPP by 60–95%.

For each case, the impact of increasing WPP on the power system transient stability is analyzed. The rate of wind power generation is assumed to be randomly variable. The rate of WPP is the rate of power generated by the wind relative to the total power delivered to the infinite bus in the base case. To perform TSA and T-D simulation, it is assumed that the time response of the system dynamics is simulated to be 20 s in the steady-state operating conditions and then the fault occurs. In this section, the fault clearing time for all cases is considered constantly to be 0.1 s. In this way, the simulations are performed and P_{DFIG} and the bus voltage of DFIG, and the rotor angle and bus voltage of SG, are monitored.

For Case A, Figs. 5 and 6 show the simulation results. According to Fig. 6a, as long as the WPP in the power system is limited to 16.67%, the grid status is stable. However, when the WPP is increased to 19.44%, the grid experiences a multi-swing rotor angle instability. Subsequently, the condition of the grid remains unstable with a higher increase (23.61% and 27.78%) in the WPP.

For Case B, simulation has been also performed in a similar way, and P_{DFIG} and the bus voltage of DFIG, as well as the bus voltage and rotor angle of SG have been monitored, the results of which are shown in Figs. 7 and 8. In this case, when the WPP increases to 33.33%, the condition of the grid is stable. However, when the WPP is increased to 38.89 and

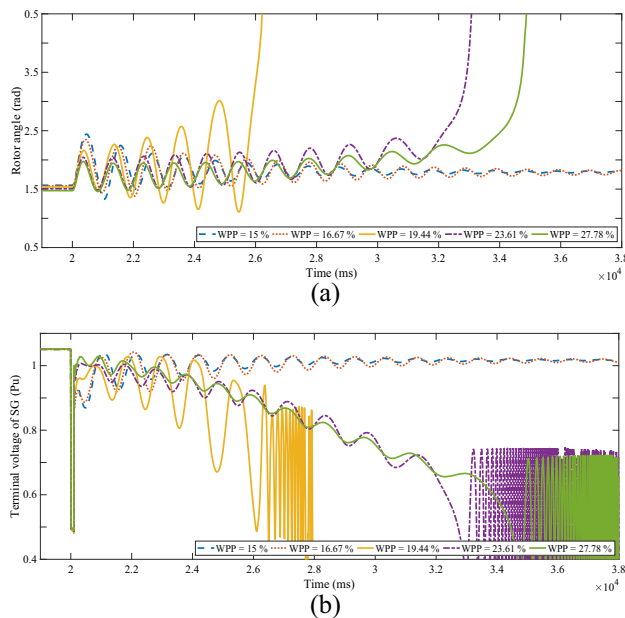


Fig. 6 The curve of the SG for Case A **a** the rotor angle and **b** the terminal voltage

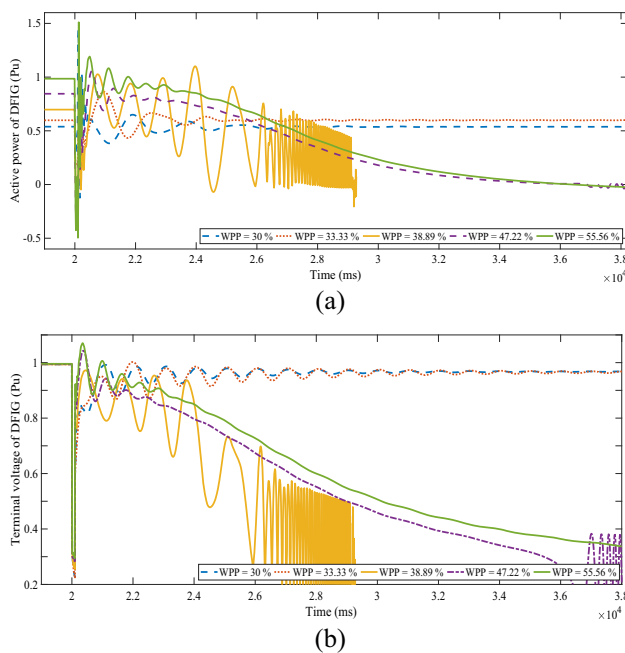


Fig. 7 The curve of the DFIG for Case B **a** the active power and **b** the bus voltage

47.22%, the grid experiences a multi-swing rotor angle instability. According to Fig. 8a, for the rate of WPP of 55.56%, the curve of the rotor angle is separately presented. It can be observed that the system will be unstable (multi-swing) in this state due to the rotor angle increasing.

For Case C, the T-D simulation has been performed similarly by setting the fault duration of 0.1 s and the results

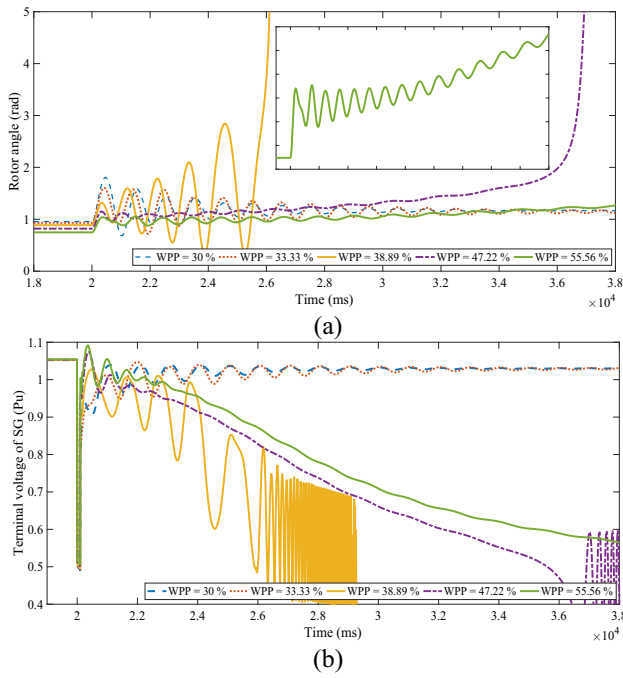


Fig. 8 The curve of the SG for Case B **a** the rotor angle and **b** the bus voltage

obtained are illustrated in Figs. 9 and 10. According to Fig. 10a, when the WPP increases to a certain threshold (66.67%), the transient stability status is suitable. However, when WPP continues to increase, the grid experiences transient instability and severe voltage drop.

To analyze the results obtained, the CCT is obtained employing T-D simulation, as given in Table 1. According to Table 1, two points can be understood. First, for each case, when the WPP is increased, the CCT also is increased in comparison with the base case condition. Thus, the condition of transient stability initially improves. By continuing to increase the WPP up to a pre-specified threshold value, the CCT is still increasing. Then, the CCT is decreased with the continuation of the increase in WPP. Accordingly, the condition of transient stability initially improves with increasing the WPP, but then the situation subsequently deteriorates. The important point here is that in each of three cases, when the rate of the power generated by the WF is limited to about 0.7 per-unit (a certain threshold), the CCT increases with the increased WPP in the system. However, when the rate of wind power generation exceeds 0.7 per-unit, the trend is reversed and the CCT decreases greatly with the increased WPP.

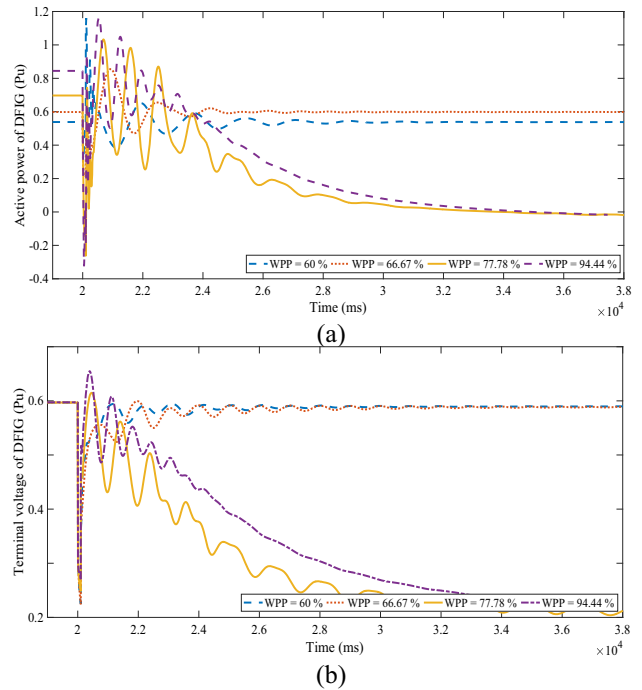


Fig. 9 The curve of the DFIG for Case C: **a** the active power and **b** the bus voltage

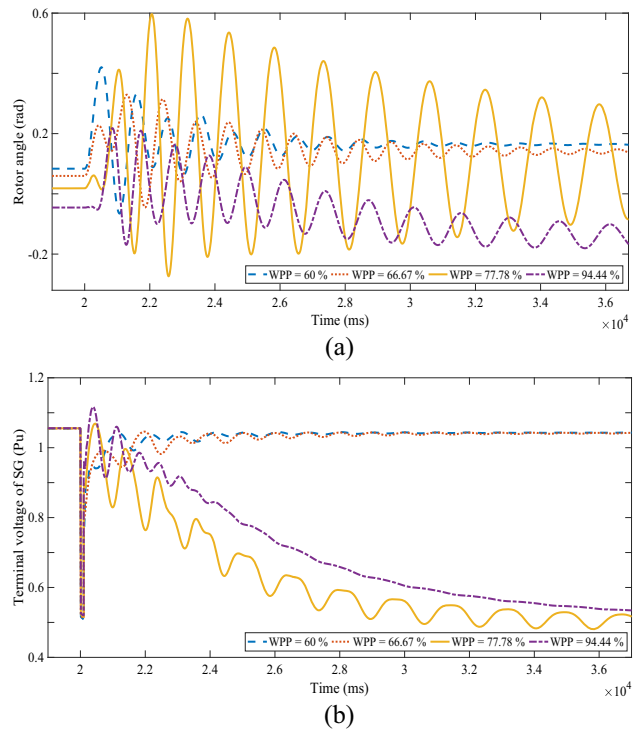


Fig. 10 The curve of the SG for Case C: **a** the rotor angle and **b** the bus voltage

Table 1 Comparison of the CCT with increasing the WPP

Cases	S_b (MVA)	Q_t (Pu)	P_t (Pu)	WPP (%)	CCT (s)	Instability type
Base case	2220	0.436	0.9	0	0.126–0.127	First swing
Case A	555	1.744	3.6	15	0.153–0.154	First swing
				16.67	0.174–0.175	First swing
				19.44	0.057–0.058	Multi-swing
				23.61	0.02–0.03	Multi-swing
				27.78	0.01–0.02	Multi-swing
Case B	1110	0.872	1.8	30	0.191–0.192	First swing
				33.33	0.270–0.271	First swing
				38.89	0.043–0.044	Multi-swing
				47.22	0.025–0.035	Multi-swing
				55.56	0.02–0.03	Multi-swing
Case C	2220	0.436	0.9	60	0.287–0.288	First swing
				66.67	0.145–0.146	Multi-swing
				77.78	0.04–0.05	Multi-swing
				94.44	0.03–0.04	Multi-swing

Second, due to the lower inertia of a DFIG compared to a SG, the higher the wind power generation in the grid, the higher the grid oscillations caused by disturbance. According to the last row of Table 1, when the rate of the power generated by the WF is limited to about 0.7 per-unit, first-swing transient instability occurs due to the insufficient synchronizing torque in the power system. However, when the rate of wind power generation exceeds 0.7 per unit, multi-swing transient instability occurs due to the insufficient damping torque. It should be noted that the rated rotor speed of DFIG is considered to be 1.2 per-unit, and it is assumed that DFIG has no reactive power exchange with the grid.

3.2 Reactive power change analysis

In this section, the effect of Q_{DFIG} has been investigated on the transient stability status. Since voltage recovery after fault clearing by a DFIG is weaker than a SG, the value of Q_{DFIG} is a vital issue in terms of TSA [11]. To do this, in all cases, the rate of reactive power generated by DFIG is increased to 0.9 per-unit. It is assumed that the short circuit fault is the same as in Sect. 3.1. Accordingly, CCT has been calculated based on TSA and T-D simulation. The simulation results obtained in this section are presented in Fig. 11. According to Fig. 11, for all cases, CCT increases when Q_{DFIG} is increased; hence, the transient stability status has been improved. Also, as in the previous subsection, when the WPP increases up to a certain threshold value, the CCT also increases, but then the situation deteriorates. As Q_{DFIG} increases, the stator and rotor currents increase. Accordingly, considering the rates of Q_{DFIG} in three different states of -0.5, 0, and 0.5 per-unit, the curves of the

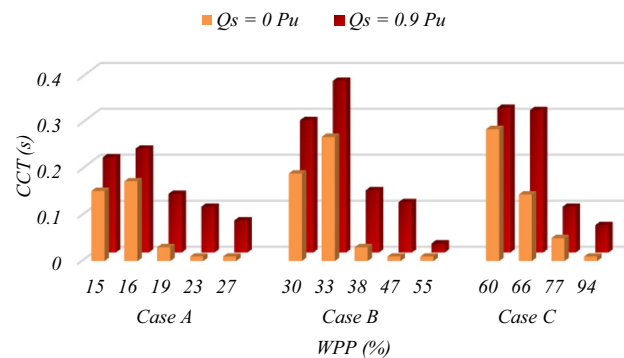


Fig. 11 The impact of the increase of reactive power generated by DFIG on CCT

rotor and stator current in the steady-state for the rated and sub-rated regimes are shown in Fig. 12.

As Fig. 12 demonstrates, when Q_{DFIG} of 0.5 per-unit, the stator current, especially the rotor current, increases significantly in both regimes. On the other hand, to decrease the power electronic converter rating, it is usually assumed that DFIG has no reactive power exchange with the grid [27, 44]. Thus, if the aim is to increase Q_{DFIG} to improve its transient stability, the steady-state rotor current of DFIG and thus the converter rating must be increased. Generally, the reactive power can be injected into the grid by DFIG in two ways [44]: Scenario A: It is assumed that no portion of the reactive power is supplied by the rotor. In this way, the GSC operates at unity power factor, and all reactive power is transferred from the stator to the grid. As stated in Sect. 2, the equivalent circuit presented for DFIG in this paper has been obtained

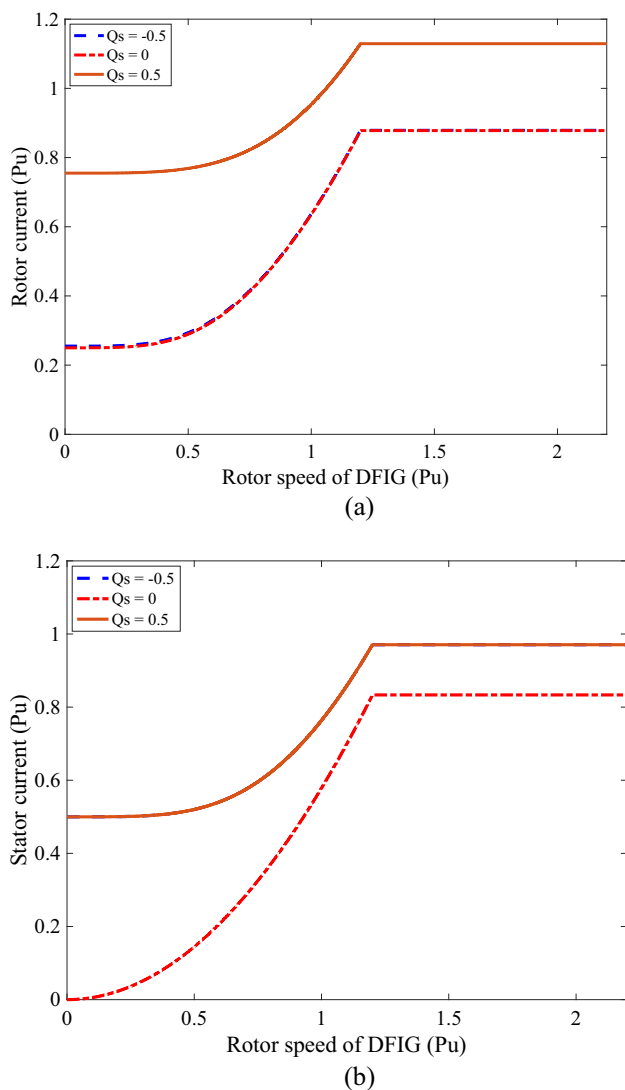


Fig. 12 The magnitude of DFIG **a** rotor and **b** stator currents in the steady state

accordingly. Scenario B: In this state, a part of the DFIG reactive power is supplied by the GSC, and therefore, the GSC does not operate at unity power factor.

In Scenario A, it is assumed that all the reactive power generated by DFIG that is equal to 0.9 per-unit is supplied by the stator, and the steady-state rotor current is considered. Here also, the conditions of the fault in the power system are the same as in the previous section. Figure 13 shows the rotor current of DFIG for all cases. As can be seen, the steady-state rotor current has increased between 21 and 33% for all three cases. Additionally, the lower the capacity of the WF, the greater the increase in rotor current due to the increase in the generated reactive power. Thus, the RSC rating should be increased in this state. On the other hand, in this state, all the generated reactive power is supplied by the DFIG stator and is injected into the grid. Therefore, the GSC operates at

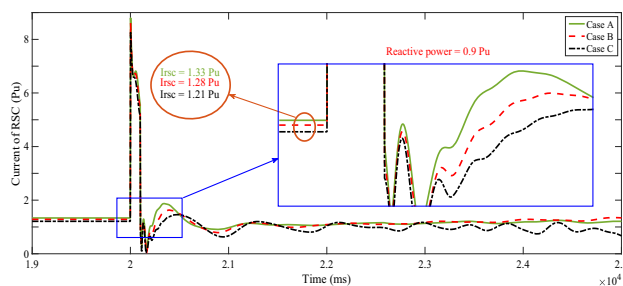


Fig. 13 The steady-state RSC current for all cases with maximum power capture of WF

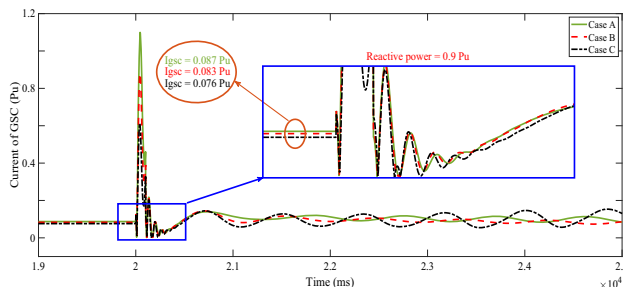


Fig. 14 The steady-state GSC current for all cases with maximum power capture of the WF

unity power factor. In Fig. 14, the GSC current for all cases is shown. Considering Fig. 14, the GSC current is very low in this state. Therefore, regarding the converter rating, this state of supplying the reactive power by DFIG does not increase the rate of the GSC.

In Scenario B, the GSC does not operate at unity power factor and supplies a part of the reactive power generated by DFIG in the operating conditions of reactive power control. Accordingly, the reactive power of the GSC is no longer equal to zero.

$$P_{GSC} = P_r, \quad Q_{GSC} = \alpha Q_{tot}; \quad \alpha \neq 0 \Rightarrow Q_{GSC} \neq 0 \Rightarrow Q_s = (1 - \alpha)Q_{tot}$$

Therefore, in this state, the GSC current changes as Eq. (19) and is placed in the equivalent circuit of DFIG:

$$I_{GSC} = \frac{P_{GSC} - jQ_{GSC}}{-jV_{qs}} \tag{19}$$

Thus, it is assumed in this section that the reactive power of 0.3 per-unit is supplied by the GSC and the reactive power of 0.6 per-unit is supplied by the stator, totally constituting the reactive power of 0.9 per-unit generated by DFIG. Figures 15 and 16 show the RSC and GSC current. In this state, the RSC current increases by about 13% and includes a less percentage of increase than Scenario A, while the GSC current includes a more percentage of increase than in Scenario A and increases by 26.8% in Case A.

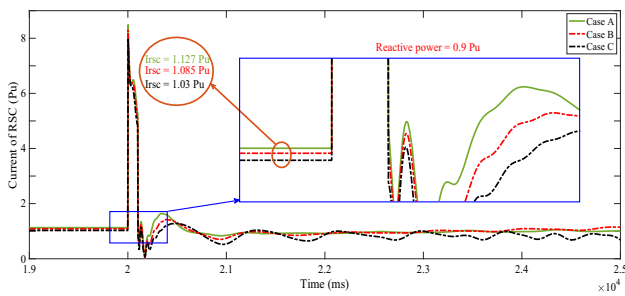


Fig. 15 The steady-state RSC current for all cases with maximum power capture of WF

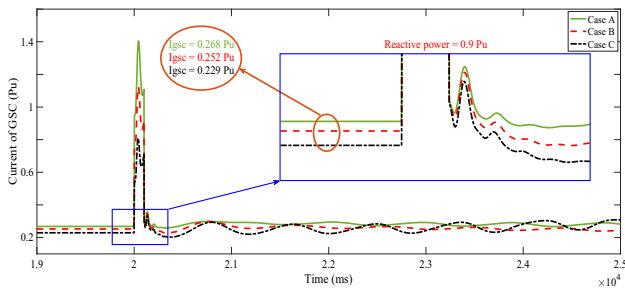
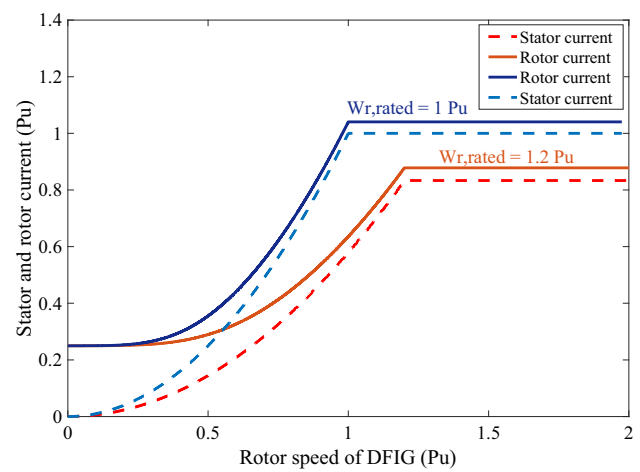


Fig. 16 The steady-state GSC current for all cases with maximum power capture of WF

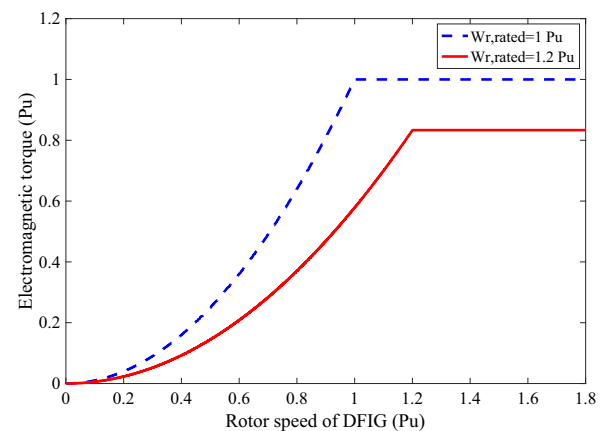
Reference [42] is one of the works conducted in this area. In [42], the impact of Q_{DFIG} on the transient stability status has been investigated and it only shows that the generation of reactive power by DFIG has a desirable impact on transient stability. In this subsection, according to what is stated above, the impact of Q_{DFIG} on the transient stability status improvement was comprehensively investigated. Based on the results of the simulations, the generation of reactive power by DFIG has a desirable impact on transient stability. However, considering how DFIG supplies reactive power in both scenarios, the increased current in the rotor can be seen, leading to an increase in the converter rating. Thus, one of the solutions proposed in this paper to prevent the increase in the converter rating can be the use of external reactive power compensation devices in the DFIG bus.

3.3 Rated rotor speed change analysis

The rated rotor speed can be chosen arbitrarily by adjusting the gearbox ratio, and the rated rotor speed has a significant impact on the electrical torque and machine currents, but due to the small amplitude, it has little impact on the rotor voltage. As mentioned earlier, in terms of the converter rating, higher value of rated rotor speed is better because it will create less the amplitude of the machine currents [44]. Accordingly, in the all of previous sections, the rated rotor speed of DFIG is considered to be 1.2 per-unit. On the other hand, it should



(a)



(b)

Fig. 17 The stator and rotor currents and the electromagnetic torque with different rated rotor speed

be noted that choosing higher rated rotor speed results in lower electrical torque. This is an issue that in the previous studies have not addressed it. Figure 17 shows the impact of changing the rated rotor speed by performing the steady-state simulation for DFIG.

As can be seen in Fig. 17, by decreasing the rated rotor speed to 1 per-unit, the currents of DFIG increase in the steady state and the condition deteriorates with respect to the converter rating. However, due to the impact of the rated rotor speed on the electromagnetic torque, the impact of changing the rated rotor speed of the DFIG on power system transient stability is studied in this section, which is considered the main contribution of this paper. For this purpose, the rated rotor speed is reduced from 1.2 per-unit to 1 per-unit by changing the gearbox ratio for all three cases and TSA is performed. Also, it is assumed that the fault of the power system is the same as in Sect. 3.1, and the time response of the system dynamics is simulated to be 20 s in the steady-state operating conditions and then the fault occurs. The fault

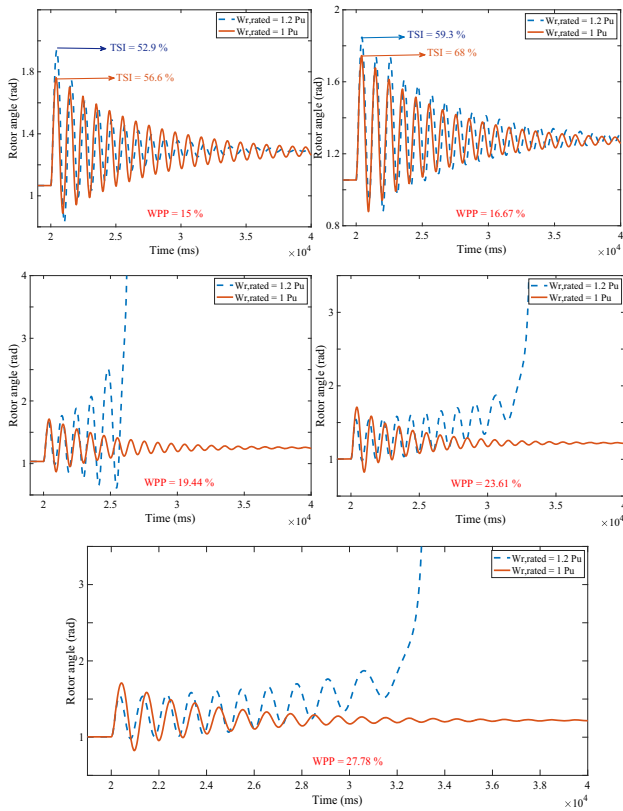


Fig. 18 The rotor angle of the SG with the change of the DFIG rated rotor speed for Case A

clearing time for all cases is considered constantly to be 0.1 s. Here, the transient stability index (TSI) is used to compare the transient stability conditions. The TSI is shown below (Eq. (20)) [42]. According to Eq. (20), the transient stability status of the system is stable when the value of η is ($\eta > 0$).

$$\eta = \frac{360 - \rho_{\max}}{360 + \rho_{\max}} \times 100 \tag{20}$$

Accordingly, simulation is performed for Case A and the rotor angle of SG for different rates of WPP is shown in Fig. 18. When the rate of WPP is equal to 15 and 16.67%, the grid is generally stable with a fault clearing time of 0.1 s. In this state, by setting the rated rotor speed to be 1 per-unit, the value of TSI will be greater than the rated rotor speed of 1.2 per-unit, leading to the improvement in the stability margin. Additionally, with the increase in WPP, it can be observed that the condition of the grid changes from unstable to stable by changing the rated rotor speed from 1.2 to 1 per-unit. Therefore, according to the results obtained, when the rated rotor speed is set to be 1 per-unit, the transient stability condition improves with the increase in the WPP.

Similarly, the simulation is performed for Case B with a constant fault clearing time of 0.1 s, and the rotor angle of SG is presented in Fig. 19. As demonstrated in Fig. 19, when the

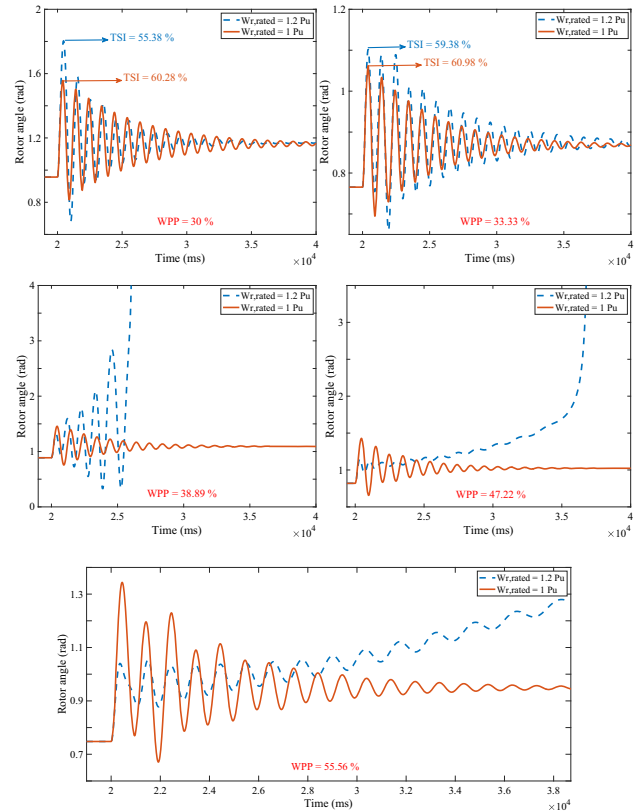


Fig. 19 The rotor angle of the SG with the change of the DFIG rated rotor speed for Case B

rate of WPP is equal to 30 and 33.33%, the grid is generally stable and by setting the rated rotor speed to be 1 per-unit, the value of TSI will be greater than the rated rotor speed of 1.2 per-unit. As a result, in this state, the stability margin is improved by decreasing the rated rotor speed. Additionally, with the increase in WPP, it can be seen that the grid condition changes from unstable to stable by changing the rotor rate speed from 1.2 to 1 per-unit. Therefore, as the results obtained indicate, when the rated rotor speed is set to be 1 per-unit, the transient stability condition also improves with the increase in the WPP.

Finally, the simulation for Case C is performed, and the rotor angle of SG is shown in Fig. 20. According to Fig. 20, in all simulated states, when the WPP increases, the value of the TSI increases by setting the rated rotor speed to be 1 per-unit, causing the grid condition to improve the transient stability status.

Therefore, as the simulation results indicate, in all cases, the transient stability condition improves by decreasing the rated rotor speed from 1.2 to 1 per-unit. Accordingly, when the rated rotor speed is equal to 1.2 per-unit, the amplitude of the rotor currents is somewhat smaller and the condition is better with regard to the converter rating, while it is not desirable in terms of transient stability. However, when the

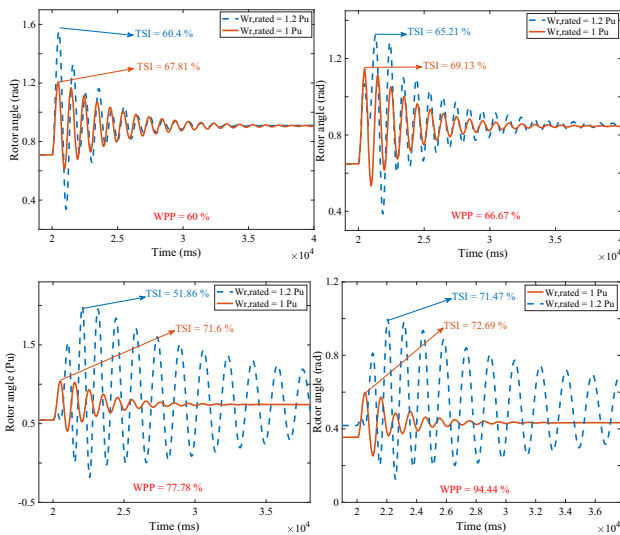


Fig. 20 The rotor angle of the SG with the change of the DFIG rated rotor speed for Case C

rated rotor speed is equal to 1 per-unit, the transient stability condition improves, while the converter rating increases somewhat. Therefore, the gearbox ratio can be considered as a parameter affecting the transient stability due to its impact on changing the value of the rated rotor speed of DFIG.

3.4 Effect of the power system strength and DFIG parameters

The power system strength as an influential parameter in transient stability studies has been analyzed in this section. The main power system presented in Fig. 4 has been considered as a weak electrical grid due to the large electrical distance, the transmission line reactance, between PCC and the power grid. In this subsection, in order to investigation of the power system strength effect, the electrical distance has been decreased in several steps. Here, the fault characteristics in the power system are the same as in the previous section. Accordingly, CCT is obtained using TSA for each of the cases, and the results are shown in Fig. 21.

For Cases A and B, when the rate of WPP is low in a weak power system, the CCT is higher. Also, when the rate of WPP in the power system increases, the CCT will increase because the power system strength has been increased. As shown in Fig. 21, for Case C, as the results obtained indicate, the value of CCT increases generally by decreasing the value of the transmission line reactance and thus strengthening the power grid. Therefore, the transient stability condition improves. However, in this state, the lower the WPP, the greater the CCT. Accordingly, based on the simulation results in this subsection, when the power system strength is increased, the transient stability status generally will improve.

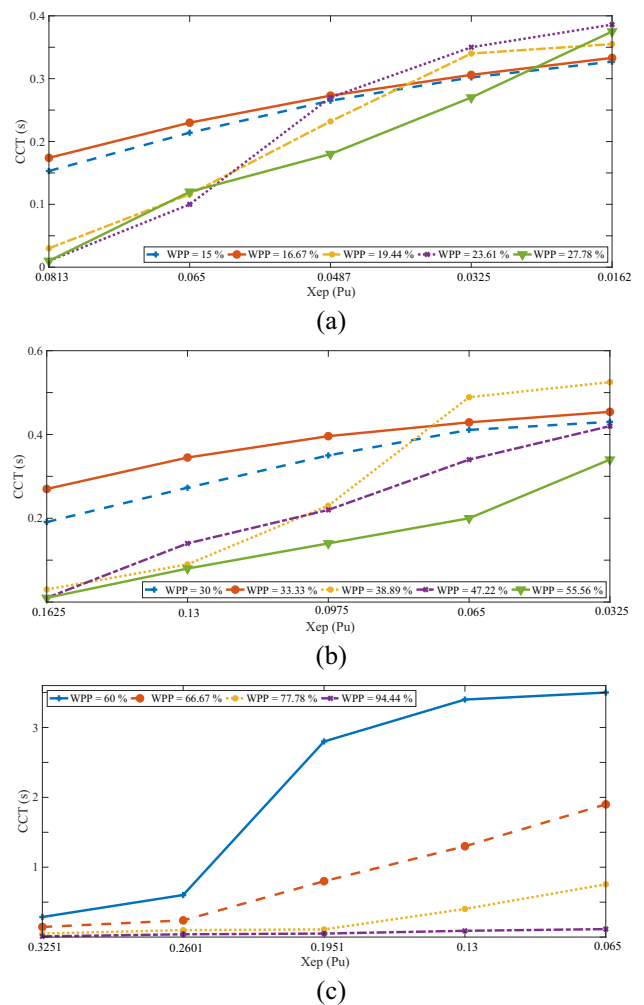


Fig. 21 The CCT curve with changing of the power system strength: **a** Case A, **b** Case B, **c** Case C

In the final part, the purpose is to investigate the effect of the DFIG parameters on transient stability by increasing the WPP. In the previous works, the effect of DFIG inertia as an effective parameter on transient stability has been investigated. It should be noted that DFIG inertia plays a crucial role in power system transient stability. Higher inertia provides enhanced system stability by contributing to the inertial response during disturbances and mitigate voltage and frequency deviations [44]. However, according to the simulations performed, the effect of DFIG stator resistance on power system transient stability is analyzed in this paper. Accordingly, to perform the simulations in this section, all of the DFIG parameters are kept constant, and we only set the stator resistance of the DFIG in 3 different steps equal to 0.005, 0.01 and 0.05 Ω. In this way, TSA is done for all cases and the CCT is calculated. Based on the simulation results in Table 2, the CCT is increased with increasing the value of the DFIG stator resistance; hence, the transient stability

Table 2 Comparison of the CCT with increasing the DFIG stator resistance

Cases		Case A													
WPP (%)	15	16.67	19.44	23.61	27.78										
r_s	0.05	0.01	0.005	0.05	0.01	0.005	0.05	0.01	0.005	0.05	0.01				
CCT (s)	0.179–0.18	0.164–0.165	0.153–0.154	0.195–0.196	0.185–0.186	0.174–0.175	0.229–0.23	<	0.057–0.058	0.23–0.24	<	0.02–0.03	0.24–0.25	<	0.01–0.02
								0.1			0.1				0.1
Cases		Case B													
WPP (%)	30	33.33	38.89	47.22	55.56										
r_s	0.05	0.01	0.005	0.05	0.01	0.005	0.05	0.01	0.005	0.05	0.01				
CCT (s)	0.268–0.269	0.208–0.209	0.191–0.192	0.311–0.312	0.29–0.291	0.27–0.271	0.32–0.33	<	0.043–0.044	0.29–0.3	0.09–0.1	0.025–0.035	0.36–0.37	0.1–0.11	0.02–0.03
								0.1							
Cases		Case C													
WPP (%)	60	66.67	77.78	94.44											
r_s	0.05	0.01	0.005	0.05	0.01	0.005	0.05	0.01	0.005	0.05	0.01				
CCT (s)	0.775–0.776	0.386–0.387	0.287–0.288	0.7–0.8	0.18–0.19	0.145–0.146	0.85–0.88	0.4–0.5	0.04–0.05	0.6–0.7	0.33–0.34	0.03–0.04			

condition improves. Therefore, the DFIG stator resistance is one of the effective parameters on transient stability.

4 Conclusion

A comprehensive analysis of the influence of the effective parameters on transient stability of the power system is covered in this paper. At first, this work has been carried out by considering the penetration of the DFIG-based WFs, the reactive power compensation by DFIG, and as well as the gearbox ratio as important factors affecting transient stability. The simulation results indicate that when the rate of the power generated by the DFIG WF is limited to about 0.7 per-unit, the CCT increases with the increased WPP in the system. However, when the rate of wind power generation exceeds 0.7 per-unit, the trend is reversed and the CCT decreases greatly with the increased WPP. Also, the simulation results show that reactive power compensation by DFIG has a desirable impact on transient stability. However, according to how reactive power is provided by DFIG, the rotor current increases, leading to an increase in the converter rating. Thus, one of the solutions proposed in this paper to prevent the increase in the converter rating can be the usage of external reactive power compensation devices in the DFIG bus. Also, according to the simulation results in all studied cases, the transient stability power system condition is improved by decreasing the rated rotor speed from 1.2 to 1 per-unit. Finally, other parameters considered for TSA are the power system strength and the stator resistance of the DFIG. As the simulation results indicate, the CCT is increased with increasing the power system strength and the value of the DFIG stator resistance; hence, the transient stability condition improves. Future work is under way by the authors to further enhance the proposed approach. The authors intend to analyze the proposed approach in a multi-machine system and investigate its challenges in practical applications.

Supplementary Information The online version contains supplementary material available at <https://doi.org/10.1007/s00202-023-01906-3>.

Author contributions HRS did conceptualization, formal analysis, investigation, methodology, project administration, resources, software, supervision, validation, visualization, writing—original draft. AH done conceptualization and supervision. MK performed conceptualization, formal analysis, and supervision. ML was involved in validation, visualization, writing—original draft. MN done writing—original draft, writing—review and editing.

Funding Open access funding provided by Aalborg University Library. The authors did not receive support from any organization for the submitted work.

Data availability The data used to support the findings of this study are available from the corresponding author upon request.

Declarations

Ethical approval This declaration is “not applicable”.

Competing interests The authors declare that they have no known competing interests.

Open Access This article is licensed under a Creative Commons Attribution 4.0 International License, which permits use, sharing, adaptation, distribution and reproduction in any medium or format, as long as you give appropriate credit to the original author(s) and the source, provide a link to the Creative Commons licence, and indicate if changes were made. The images or other third party material in this article are included in the article’s Creative Commons licence, unless indicated otherwise in a credit line to the material. If material is not included in the article’s Creative Commons licence and your intended use is not permitted by statutory regulation or exceeds the permitted use, you will need to obtain permission directly from the copyright holder. To view a copy of this licence, visit <http://creativecommons.org/licenses/by/4.0/>.

Appendix A

The parameters of the aggregated model of the DFIG WF and the SMIB system in per-unit are given as Table 3 (base power is 2220 MVA).

Table 3 The parameters of the SMIB system understudy

The SG and excitation system		The SMIB system		The DFIG wind farm	
f_B	60(Hz)	V_s	0.90081(Pu)	L_m	4 (Pu)
X_d	1.81(Pu)	θ_s	0(deg)	L_{ss}	1.01 L_m (Pu)
X_q	1.76(Pu)	X_{t1}	0.15(Pu)	L_{rr}	1.005 L_{ss} (Pu)
X'_d	0.3(Pu)	X_{t2}	0.04(Pu)	r_s	0.005(Pu)
X'_q	0.65(Pu)	X_{e1}	0.5(Pu)	r_r	1.1 r_s (Pu)
R_s	0.003(Pu)	X_{e2}	0.93(Pu)	H_f	4(s)
H	3.5(s)	P_f	0.9(Pu)	H_g	0.1 H_f (s)
D	0	Q_f	0.436(Pu)	K	0.3(Pu/el.rad)
T'_{d0}	8(s)			C	0.01(Pu.s/el.rad)
T'_{q0}	1(s)			β	0
K_A	2			V_w	15(m/s)
T_A	0.015(s)			$P_{tw, rated}$	5(MW)
				R	40.05(m)
				ρ	1.225(kg/m ³)

References

- Mansouri SA, Jordehi AR, Marzband M, Tostado-Véliz M, Jurado F, Aguado JA (2023) An IoT-enabled hierarchical decentralized framework for multi-energy microgrids market management in the presence of smart prosumers using a deep learning-based forecaster. *Appl Energy* 333:120560
- Mansouri SA, Nematbakhsh E, Jordehi AR, Marzband M, Tostado-Véliz M, Jurado F (2023) An interval-based nested optimization framework for deriving flexibility from smart buildings and electric vehicle fleets in the TSO-DSO coordination. *Appl Energy* 341:121062
- Mansouri SA, Nematbakhsh E, Ahmarinejad A, Jordehi AR, Javadi MS, Marzband M (2022) A hierarchical scheduling framework for resilience enhancement of decentralized renewable-based microgrids considering proactive actions and mobile units. *Renew Sustain Energy Rev* 168:112854
- Mansouri SA, Nematbakhsh E, Jordehi AR, Tostado-Véliz M, Jurado F, Leonowicz Z (2022) A risk-based bi-level bidding system to manage day-ahead electricity market and scheduling of interconnected microgrids in the presence of smart homes. In: *IEEE international conference on environment and electrical engineering and IEEE industrial and commercial power systems Europe (EEEIC/I&CPS Europe)*
- Mansouri SA, Ahmarinejad A, Sheidaei AF, Javadi MS, Rezaee Jordehi A, Esmael Nezhad A, Catalão JPS (2022) A multi-stage joint planning and operation model for energy hubs considering integrated demand response programs. *Int J Electric Power Energy Syst* 140:108103
- Mansouri SA, Nematbakhsh E, Ahmarinejad A, Jordehi AR, Javadi MS, Matin SAA (2022) A multi-objective dynamic framework for design of energy hub by considering energy storage system, power-to-gas technology and integrated demand response program. *J Energy Storage* 50:104206
- Mansouri SA, Ahmarinejad A, Nematbakhsh E, Javadi MS, Jordehi AR, Catalão JPS (2021) Energy management in microgrids including smart homes: a multi-objective approach. *Sustain Cities Soc* 69:102852
- Mansouri SA, Ahmarinejad A, Javadi MS, Nezhad AE, Shafie-Khah M, Catalão JPS (2021) Chapter 9—Demand response role for enhancing the flexibility of local energy systems. In: *Distributed energy resources in local integrated energy systems*, pp 279–313
- Mansouri SA, Ahmarinejad A, Nematbakhsh E, Javadi MS, Nezhad AE, Catalão JPS (2022) A sustainable framework for multi-microgrids energy management in automated distribution network by considering smart homes and high penetration of renewable energy resources. *Energy* 245:123228
- Renné DS (2022) Progress, opportunities and challenges of achieving net-zero emissions and 100% renewables. *Solar Compass* 1:100007
- Shabani HR, Kalantar M, Hajizadeh A (2021) Investigation of the closed-loop control system on the DFIG dynamic models in transient stability studies. *Int J Electr Power Energy Syst* 131:107084
- Shabani HR, Kalantar M, Hajizadeh A (2021) Real-time transient instability detection in the power system with high DFIG-wind turbine penetration via transient energy. *IEEE Syst J* 16(2):3013–3024
- Global Wind Energy Council (GWEC). <https://gwec.net>
- Slootweg JG, De Haan SWH, Polinder H, Kling WL (2003) General model for representing variable speed wind turbines in power system dynamics simulations. *IEEE Trans Power Syst* 18(1):144–151
- Chowdhury MA, Shen W, Hosseinzadeh N, Pota HR (2015) Transient stability of power system integrated with doubly fed induction generator wind farms. *IET Renew Power Gener* 9(2):184–194
- Mastoi MS, Tahir MJ, Usman M, Wang D, Zhuang S, Hassan M (2022) Research on power system transient stability with wind generation integration under fault condition to achieve economic benefits. *IET Power Electron* 15(3):263–274
- Liu Y, Wang J, Yue Z (2022) Improved Multi-point estimation method based probabilistic transient stability assessment for power system with wind power. *Int J Electr Power Energy Syst* 142:108283
- Hu Q, Xiong Y, Liu C, Wang G, Ma Y (2022) Transient stability analysis of direct drive wind turbine in DC-link voltage control timescale during grid fault. *Processes* 10(4):774
- Kumar AW, Mufti MUD, Zargar MY (2022) Adaptive predictive control of flywheel storage for transient stability enhancement of a wind penetrated power system. *Int J Energy Res* 46(5):6654–6671
- Hasanien HM, Tostado-Véliz M, Turkey RA, Jurado F (2022) Hybrid adaptive controlled flywheel energy storage units for transient

- stability improvement of wind farms. *Journal of Energy Storage* 54:105262
21. Bhukya J, Kumar Singh N, Mahajan V (2023) Impact of aggregated model-based optimization for wind farm and electric vehicle on power system stability. *Comput Electr Eng* 105:108480
 22. Zhang G, Zhao J, Hu W, Cao D, Tan B, Huang Q, Chen Z (2023) A novel data-driven self-tuning SVC additional fractional-order sliding mode controller for transient voltage stability with wind generations. *IEEE Trans Power Syst*
 23. Luo J, Teng F, Bu S, Chu Z, Tong N, Meng A, Yang L, Wang X (2023) Converter-driven stability constrained unit commitment considering dynamic interactions of wind generation. *Int J Electr Power Energy Syst* 144:108614
 24. Ledesma P, Usaola J (2005) Doubly fed induction generator model for transient stability analysis. *IEEE Trans Energy Convers* 20(2):388–397
 25. Ledesma P, Usaola J (2004) Effect of neglecting stator transients in doubly fed induction generators models. *IEEE Trans Energy Convers* 19(2):459–461
 26. Muljadi E, Butterfield CP, Parsons B, Ellis A (2007) Effect of variable speed wind turbine generator on stability of a weak grid. *IEEE Trans Energy Convers* 22(1):29–36
 27. Chowdhury MA, Shen WX, Hosseinzadeh N, Pota HR (2015) A review on transient stability of DFIG integrated power system. *Int J Sustain Eng* 8(6):405–416
 28. Katsivelakis M, Bargiotas D, Daskalopulu A (2020) Transient stability analysis in power systems integrated with a doubly-fed induction generator wind farm. In: 2020 11th international conference on information, intelligence, systems and applications (IISA). IEEE, pp 1–7
 29. Soued S, Ramadan HS, Becherif M (2019) Effect of doubly fed induction generator on transient stability analysis under fault conditions. *Energy Procedia* 162:315–324
 30. Ghaedi S, Abazari S, Arab Markadeh G (2022) Novel non-linear control of DFIG and UPFC for transient stability increment of power system. *IET Gener Transm Distrib* 16(19):3799–3813
 31. Atallah M, Mezouar A, Belgacem K, Benmahdjoub MA, Saidi Y, Brahmi B (2022) Grid synchronization of equivalent wind farm equipped with DFIG model for transient stability by using nonlinear integral backstepping control. *Arab J Sci Eng* 48:5771–5783
 32. Baimel D, Chowdhury N, Belikov J, Levron Y (2021) New type of bridge fault current limiter with reduced power losses for transient stability improvement of DFIG wind farm. *Electric Power Syst Res* 197:107293
 33. Bhukya J, Naidu TA, Vuddanti S, Konstantinou C (2021) Coordinated control and parameters optimization for PSS, POD and SVC to enhance the transient stability with the integration of DFIG based wind power systems. *Int J Emerg Electr Power Syst* 23(3):359–379
 34. Abazari S, Ghaedi S (2022) Transient stability increase of multi-machine power system by using SSSC and DFIG control with TEF technique and super twisting differentiator. *ISA Trans* 136:390–399
 35. Shabani HR, Kalantar M (2021) Real-time transient stability detection in the power system with high penetration of DFIG-based wind farms using transient energy function. *Int J Electr Power Energy Syst* 133:107319
 36. Xu P, Zhao W, Li F (2022) Transient stability analysis method of grid-connected DFIG based on direct method. In: 2022 4th International conference on electrical engineering and control technologies (CEEECT). IEEE, pp 675–679
 37. Camargo RS, Amorim AEA, Bueno EJ, Encarnação LF (2021) Novel multilevel STATCOM for power system stability enhancement on DFIG-based wind farms. *Electric Power Syst Res* 197:107316
 38. Musarrat MN, Fekih A (2021) A fractional order sliding mode control-based topology to improve the transient stability of wind energy systems. *Int J Electr Power Energy Syst* 133:107306
 39. Fdaili M, Essadki A, Kharchouf I, Nasser T (2021) Noncontrolled fault current limiter with reactive power support for transient stability improvement of DFIG-based variable speed wind generator during grid faults. *Int Trans Electr Energy Syst* 31(8):e12955
 40. Akanto JM, Hazari MR, Mannan MA (2021) LVRT and stability enhancement of grid-tied wind farm using DFIG-based wind turbine. *Appl Syst Innov* 4(2):33
 41. Hossain ME (2017) A non-linear controller based new bridge type fault current limiter for transient stability enhancement of DFIG based Wind Farm. *Electric Power Syst Res* 152:466–484
 42. Edrah M, Lo KL, Anaya-Lara O (2015) Impacts of high penetration of DFIG wind turbines on rotor angle stability of power systems. *IEEE Trans Sustain Energy* 6(3):759–766
 43. Munkhchuluun E, Meegahapola L, Vahidnia A (2020) Impact of active power recovery rate of DFIG wind farms on first swing rotor angle stability. *IET Gener Transm Distrib* 14(25):6041–6048
 44. Mei F (2008) Small-signal modelling and analysis of doubly-fed induction generators in wind power applications
 45. Shankar R, Kundur P (1994) *Power system stability and control II*. McGraw-Hill Books, New York, p 581
 46. Sauer PW, Pai MA (1998) *Power system dynamics and stability*. Prentice-Hall, Upper Saddle River
 47. Mei F, Pal B (2007) Modal analysis of grid-connected doubly fed induction generators. *IEEE Trans Energy Convers* 22(3):728–736
 48. Mitra A, Chatterjee D (2013) A sensitivity based approach to assess the impacts of integration of variable speed wind farms on the transient stability of power systems. *Renew Energy* 60:662–671
 49. Ekanayake JB, Holdsworth L, Wu X, Jenkins N (2003) Dynamic modeling of doubly fed induction generator wind turbines. *IEEE Trans Power Syst* 18(2):803–809
 50. Mitra A, Chatterjee D (2015) Active power control of DFIG-based wind farm for improvement of transient stability of power systems. *IEEE Trans Power Syst* 31(1):82–93
 51. Lei Y, Mullane A, Lightbody G, Yacamini R (2006) Modeling of the wind turbine with a doubly fed induction generator for grid integration studies. *IEEE Trans Energy Convers* 21(1):257–264

Publisher's Note Springer Nature remains neutral with regard to jurisdictional claims in published maps and institutional affiliations.